THE JOURNAL OF PHYSICAL CHEMISTRY B

Article

pubs.acs.org/JPCB

Simulation of Two-Dimensional Sum-Frequency Generation Response Functions: Application to Amide I in Proteins

Chungwen Liang[†] and Thomas L. C. Jansen*[,‡]

[†]Biozentrum, University of Basel, Klingelbergstrasse 50/70, CH - 4056 Basel, Switzerland

[‡]Zernike Institute for Advanced Materials, University of Groningen, Nijenborgh 4, 9747 AG Groningen, The Netherlands

ABSTRACT: We present the implementation of an approach to simulate the two-dimensional sum frequency generation response functions of systems with numerous coupled chromophores using a quantum-classical simulation scheme that was previously applied successfully to simulate two-dimensional infrared spectra. We apply the simulation to the amide I band of a mechanosensitive channel protein. By examining the signal generated from different segments of the protein, we find that the overall signal is impossible to interpret without the aid of simulations due to the interference of the response generated on different segments of the protein. We do not find significant cross-peaks in the spectra, even when the waiting time is increased. The spectra are thus not sensitive to coupling between different structural elements. Despite this, we conclude that two-dimensional sum frequency generation spectroscopy will be a powerful tool to investigate membrane bound proteins.

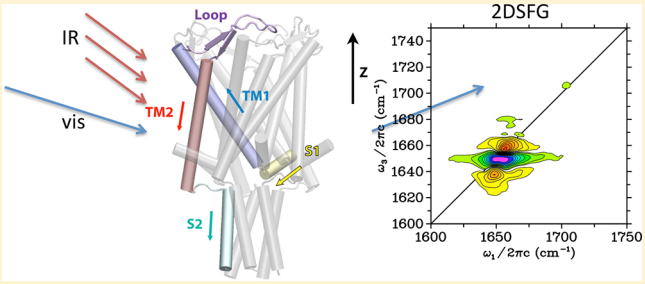

INTRODUCTION

Sum-frequency generation (SFG)[1,2] is a powerful technique to study the structure of interfaces as the signal from bulk centrosymmetric materials vanishes in this second-order technique. Recently, this method has been extended to the fourth-order two-dimensional sum-frequency generation (2DSFG) technique[3,4] in a similar manner as the two-dimensional infrared (2DIR)[5] and two-dimensional electronic[6] spectroscopies were recently developed. All of these optical techniques were inspired by the development of multidimensional nuclear magnetic resonance (NMR) techniques.[7] The most significant advantages of all these optical techniques is that they allow studying dynamics on a sub-picosecond time scale[8−16] due to the introduction of a variable waiting time and they are sensitive to structure due to the presence of cross-peaks.[5,17−20] 2DSFG is still in its infancy, and so far, it has only been applied to very few systems.[3,4,21−24] Due to spectral congestion and interference between signal contributions very much like in 2DIR, the spectra can generally be expected to be difficult to interpret. In 2DSFG, the sign of the signals depends on the molecular orientation;[25] therefore, additional complications in the interpretation can be expected as compared to 2DIR. For the successful application of 2DSFG, it will be crucial that theoretical methods to simulate the spectra are developed. So far, the theoretical treatment has been limited to a few studies.[3,25,26] In this paper, we will extend the quantum-classical approach often denoted as the numerical integration of the Schrödinger equation (NISE) scheme[16,27−29] to allow the calculation of the 2DSFG response functions governing the 2DSFG signals for multichromophoric systems.

The ability to selectively study surfaces has made the SFG technique[1,2] popular. It has been extensively used for studying liquid interfaces.[30,31] The study of peptides and proteins at surfaces has recently been done as well, including studies on the amide I.[32−34] For proteins, the SFG technique is particularly interesting, as it is suited for the study of membrane bound proteins. Resolving the structure of such proteins is generally very challenging with the well-established X-ray and NMR techniques. Therefore, the structure is only known for a few hundred membrane proteins. Membrane proteins include most important drug targets as any drug needs to either act at the bacterial membrane, viral surface or penetrate this. Membrane proteins are thus important targets for alternative structural probes as SFG. The amide I region is a good target, as the transition dipole is strong, which both provides a strong signal and strong coupling, making the amide I band sensitive to structure.[35−37] For vibrational spectroscopy studies on the amide I band in the presence of water, the water bend is located essentially at the same frequency as the amide I vibration. This water bend is experimentally eliminated using heavy water as solvent. This also results in an exchange of the acidic proton in the peptide unit, slightly changing the amide I frequency. This is also a well-known trick used in absorption and 2DIR spectroscopies of the amide I band. So far, the amide I band has not been subject to 2DSFG studies. Such application will open for more detailed structural studies of membrane embedded proteins with the combined advantages from going to a two-dimensional spectroscopy and the surface, and directional sensitivity of the SFG technique. The possible presence of cross-peaks and the ability to vary the waiting time and study dynamical properties as spectral diffusion will open for new possibilities of studying membrane bound proteins.

Received: March 29, 2013
Revised: May 3, 2013
Published: May 8, 2013

   dx.doi.org/10.1021/jp403111j | J. Phys. Chem. B 2013, 117, 6937−6945

Modeling of 2DSFG spectra of multi-chromophoric systems like the amide I vibrations of proteins embedded in a complex environment like a membrane is very challenging. First of all, one needs to achieve a reliable model of the structure. This can presumably be done using an X-ray or NMR starting structure if available or if the structure is not known predicting the most probable structure using protein folding simulations.[38] The structural fluctuations can then be determined by inserting the structure in the desired membrane in a molecular dynamics simulation. Assuming that this is achieved, the next problem is to determine the desired parameters defining the spectra, i.e., as the vibrational frequencies and absorption strengths.[39−44] As this is done, a procedure for actually calculating the spectra is needed. In the first 2DSFG papers, this was done by essentially neglecting the dynamics of studied system.[3,25] In a more recent theoretical study of the dynamics of surface water, such an approximation could obviously not be done, as the very dynamics was the aim of the study.[26] Instead, a powerful response function based quantum-classical approach was used. This allows both accounting for the actual chemical exchange of hydrogen bonds at the water surface as well as the motional narrowing that the environmental fluctuations induce. At the same time, the non-Condon effects arising from fluctuations in the absorption cross section varying between different local environments[45,40] was to be accounted for. The implementation, however, only considered a single chromophore. When multiple chromophores are close to each other as the amide I modes of proteins, they couple, resulting in delocalized eigenstates and excitation transfer.[28,29,46] Such an effect can be accounted for by extending the theory to multi-chromophoric systems as was done for 2DIR[28,29,46] in an approach that we denote the numerical integration of the Schrödinger equation approach (NISE). This was recently optimized to be applicable to proteins with hundreds of coupled chromophores.[27]

The focus of the present paper will be to simulate the fourth-order response functions governing the 2DSFG signal. We will use the mechanosensitive channel of large conductance (MscL)[47−50] as a model system for the calculation. For calculating the response functions, we will use a new implementation of the NISE approach[16,27−29] extended to allow for the calculation of 2DSFG response functions. This will be described in the Theory section. The application to the MscL channel will be described in the Application to a Membrane Protein section, where results will be presented for the full membrane protein as well as for segments of the full system. This is followed by a Discussion section, and finally, the conclusions will be presented.

THEORY

The overall 2DSFG response is given by

$$\chi^{(4)}_{\mathrm{eff}} = \sum_{IJKLM} A_I(\Omega_{\mathrm{det}}, \gamma_{\mathrm{det}}, \omega_{\mathrm{det}}) A_J(\Omega_{\mathrm{vis}}, \gamma_{\mathrm{vis}}, \omega_{\mathrm{vis}}) \times A_K(\Omega_{\mathrm{IR3}}, \gamma_{\mathrm{IR3}}, \omega_{\mathrm{IR3}}) A_L(\Omega_{\mathrm{IR2}}, \gamma_{\mathrm{IR2}}, \omega_{\mathrm{IR2}}) \times A_M(\Omega_{\mathrm{IR1}}, \gamma_{\mathrm{IR1}}, \omega_{\mathrm{IR1}}) \chi^{(4)}_{IJKLM}(\omega_{\mathrm{det}}, \omega_{\mathrm{vis}}, \omega_{\mathrm{IR3}}, \omega_{\mathrm{IR2}}, \omega_{\mathrm{IR1}}) \quad (1)$$

where $\chi^{(4)}_{IJKLM}$ are the lab frame response functions.[25] Ω denotes the polarization angles of the four incidents beams and the detector (det). γ is the incidence angle of the beams relative to the surface normal, and ω is the frequency of the field. The angle dependent prefactors A are given in the appendix.

In the remainder of this paper, we will restrict ourselves to the lab frame polarization conditions $\chi^{(4)}_{ZZZZZ}$ and $\chi^{(4)}_{ZZZYY}$. In an idealized experiment with glancing angle incidence of the beams, this corresponds to the experiments, where all fields are p-polarized (ppppp), and where the initial infrared pulse pair has s-polarization (pppss), respectively. In the molecular dynamics frame, this corresponds to the polarization conditions $\chi^{(4)}_{zzzzz}$ and $(\chi^{(4)}_{zzzyy} + \chi^{(4)}_{zzzxx})/2$, when the sample is ordered in the surface normal direction and isotropic in the surface plane directions. In the Appendix, a table of the molecular dynamics frame to lab frame conversion is presented. For a more detailed discussion on the utilization of polarization conditions, see ref 25.

In the following, a collection of three-level systems will be considered. This is sufficient to describe 2DSFG, as one cannot reach higher excited levels with the employed laser pulses. We employ the simplest possible exciton Hamiltonian for a collection of N floating oscillators of the form

$$H(t) = \sum_{i=1}^{N}\left[\varepsilon_i(t) b_i^\dagger b_i - \frac{\Delta_i(t)}{2} b_i^\dagger b_i^\dagger b_i b_i\right] + \sum_{i,j}^{N} J_{ij}(t) b_i^\dagger b_j + \sum_{i=1}^{N} (\vec{\mu}_i(t)\cdot\vec{E}(t) + \overline{\overline{\alpha}}_i(t) : \vec{E}(t)\vec{E}(t))[b_i^\dagger + b_i] \quad (2)$$

Here $\varepsilon_i(t)$ and $\Delta_i(t)$ are the fluctuating frequency and anharmonicity, respectively, of mode i, $J_{ij}(t)$ is the fluctuating coupling between two modes, and $b_i^\dagger$ and b_i are the usual Bose creation and annihilation operators. The modes interact with the applied electric field $\vec{E}(t)$ through the transition dipoles $\vec{\mu}_i(t)$ and transition polarizabilities $\overline{\overline{\alpha}}_i(t)$, which fluctuate in time as well. The dyadic product is indicated with a colon. In the Hamiltonian (eq 2), states with a different number of excitations are only coupled when an external field is present. When the external field is vanishing, it is therefore block diagonal and the different blocks can be treated separately. We denote the block concerning the ground state H^{gg}, the single excited states H^{ee}, and the double excited states H^{ff}. We will consider interactions with an external electric field tuned to be resonant with the change of one excitation quantum. In this case, we need the transition dipoles and transition polarizabilities between the ground state and the single excited states μ^{ge} and α^{ge} and those between the single and double excited states μ^{ef} and α^{ef}.

For calculating the response functions, we will use the NISE approach.[28,29,46] This method utilizes the time-dependent perturbation theory expressions for the response functions.[51] The response functions are evaluated from a trajectory describing the evolution of the spectroscopic Hamiltonian as a function of a fluctuating environment. Such a Hamiltonian can for example be constructed by combining MD simulations and *ab initio* mappings for vibrational frequencies, anharmonicities, couplings, transition dipoles, and transition polarizabilities.[40−43,52−58] The time evolution operators in the response functions are evaluated by dividing time into small intervals in which the Hamiltonian can be seen as time-independent, and the wave function is propagated according to the solution of the time-independent Schrödinger equation. In this way, time-evolution operators, $\mathbf{U}$, for each interval can be obtained. For longer time intervals, time-evolution operators for multiple small time intervals are multiplied to obtain the time evolution.[16] The approach described here and the Hamiltonian employed allow for the description of population transfer within the exciton manifolds. Therefore, we can represent the time evolution in each manifold with the time-evolution operator in that manifold only. These are denoted $\mathbf{U}^{gg}$, $\mathbf{U}^{ee}$, and $\mathbf{U}^{ff}$. The first describes the time evolution of the ground state and equals the identity with the applied Hamiltonian and will be omitted in the equations below. The two

dx.doi.org/10.1021/jp403111j | J. Phys. Chem. B 2013, 117, 6937−6945

latter describe the time evolution of the single excited and double excited state manifolds, respectively. We used the optimization scheme described in ref 27 for the propagation during t_1 and t_3 to allow for the treatment of large systems. During the waiting time, t_2, the more accurate propagation scheme using direct diagonalization is employed.

For 2DSFG, six response functions contribute. These are the ground state bleach (GB), stimulated emission (SE), and excited state absorption (EA) contributions, which all come in a rephasing (I) and a nonrephasing (II) version.[51] These response functions can also be represented by double sided Feynman diagrams, as in Figure 1.[51,59] The equations for the six response functions are

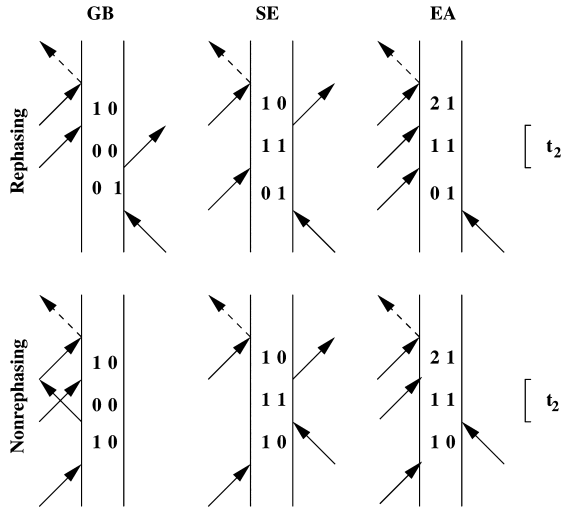

Figure 1. The six basic double sided Feynman diagrams governing the 2DSFG response.

$$\chi^{(\mathrm{I})}_{\mathrm{GB}}(t_3, t_2, t_1) = -\left(\frac{i}{\hbar}\right)^3 \langle\langle g|\mu^{ge}(\tau_1)\mathbf{U}^{ee}(\tau_1, \tau_2)\mu^{eg}(\tau_2) \times \alpha^{ge}(\tau_4)\mathbf{U}^{ee}(\tau_4, \tau_3)\mu^{eg}(\tau_3)|g\rangle\rangle_E \Gamma(t_3, t_2, t_1)$$

$$\chi^{(\mathrm{I})}_{\mathrm{SE}}(t_3, t_2, t_1) = -\left(\frac{i}{\hbar}\right)^3 \langle\langle g|\mu^{ge}(\tau_1)\mathbf{U}^{ee}(\tau_1, \tau_3)\mu^{eg}(\tau_3) \times \alpha^{ge}(\tau_4)\mathbf{U}^{ee}(\tau_4, \tau_2)\mu^{eg}(\tau_2)|g\rangle\rangle_E \Gamma(t_3, t_2, t_1)$$

$$\chi^{(\mathrm{I})}_{\mathrm{EA}}(t_3, t_2, t_1) = \left(\frac{i}{\hbar}\right)^3 \langle\langle g|\mu^{ge}(\tau_1)\mathbf{U}^{ee}(\tau_1, \tau_4)\alpha^{ef}(\tau_4) \times \mathbf{U}^{ff}(\tau_4, \tau_3)\mu^{fe}(\tau_3)\mathbf{U}^{ee}(\tau_3, \tau_2)\mu^{eg}(\tau_2)|g\rangle\rangle_E \times \Gamma(t_3, t_2, t_1)$$

$$\chi^{(\mathrm{II})}_{\mathrm{GB}}(t_3, t_2, t_1) = -\left(\frac{i}{\hbar}\right)^3 \langle\langle g|\alpha^{ge}(\tau_4)\mathbf{U}^{ee}(\tau_4, \tau_3) \times \mu^{eg}(\tau_3)\mu^{ge}(\tau_2)\mathbf{U}^{ee}(\tau_2, \tau_1)\mu^{eg}(\tau_1)|g\rangle\rangle_E \times \Gamma(t_3, t_2, t_1)$$

$$\chi^{(\mathrm{II})}_{\mathrm{SE}}(t_3, t_2, t_1) = -\left(\frac{i}{\hbar}\right)^3 \langle\langle g|\mu^{ge}(\tau_2)\mathbf{U}^{ee}(\tau_2, \tau_3)\mu^{eg}(\tau_3) \times \alpha^{ge}(\tau_4)\mathbf{U}^{ee}(\tau_4, \tau_1)\mu^{eg}(\tau_1)|g\rangle\rangle_E \Gamma(t_3, t_2, t_1)$$

$$\chi^{(\mathrm{II})}_{\mathrm{EA}}(t_3, t_2, t_1) = \left(\frac{i}{\hbar}\right)^3 \langle\langle g|\mu^{ge}(\tau_2)\mathbf{U}^{ee}(\tau_2, \tau_4)\alpha^{ef}(\tau_4) \times \mathbf{U}^{ff}(\tau_4, \tau_3)\mu^{fe}(\tau_3)\mathbf{U}^{ee}(\tau_3, \tau_1)\mu^{eg}(\tau_1)|g\rangle\rangle_E \times \Gamma(t_3, t_2, t_1) \quad (3)$$

The brackets $\langle\langle\cdots\rangle\rangle_E$ denote the average of the classical ensemble and the expectation value of the quantum system together. The vibrational lifetime is included in an *ad hoc* way through the relaxation factor

$$\Gamma(t_3, t_2, t_1) = \exp(-(t_3 + 2t_2 + t_1)/2T_1) \quad (4)$$

τ_1 through τ_4 are the times for interactions with the external electric field, and t_1 through t_3 are the time delays between these (i.e., $t_1 = \tau_2 - \tau_1$, $t_2 = \tau_3 - \tau_2$, and $t_3 = \tau_4 - \tau_3$). In this simplified treatment, all states are assumed to have the same lifetime, T_1.

The response functions are converted to the frequency domain using 2D Fourier transforms with respect to the time differences t_1 and t_3:

$$\chi^{(\mathrm{I})}(\omega_3, t_2, \omega_1) = \int_0^\infty \int_0^\infty (\chi^{(\mathrm{I})}_{\mathrm{GB}}(t_3, t_2, t_1) + \chi^{(\mathrm{I})}_{\mathrm{SE}}(t_3, t_2, t_1) + \chi^{(\mathrm{I})}_{\mathrm{EA}}(t_3, t_2, t_1)) \exp(i(\omega_3 t_3 - \omega_1 t_1))\, \mathrm{d}t_3\, \mathrm{d}t_1$$

$$\chi^{(\mathrm{II})}(\omega_3, t_2, \omega_1) = \int_0^\infty \int_0^\infty (\chi^{(\mathrm{II})}_{\mathrm{GB}}(t_3, t_2, t_1) + \chi^{(\mathrm{II})}_{\mathrm{SE}}(t_3, t_2, t_1) + \chi^{(\mathrm{II})}_{\mathrm{EA}}(t_3, t_2, t_1)) \exp(i(\omega_3 t_3 + \omega_1 t_1))\, \mathrm{d}t_3\, \mathrm{d}t_1 \quad (5)$$

t_2 is the waiting time. The final response functions used in eq 1 are given by the sum of the rephasing and nonrephasing contributions.[25,59] In all plots presented in this paper, the imaginary part of the response functions corresponding to the absorptive response is shown.

APPLICATION TO A MEMBRANE PROTEIN

We applied the 2DSFG simulation to the closed state of MscL.[47] This protein consists of five identical chains (see Figure 2). Each

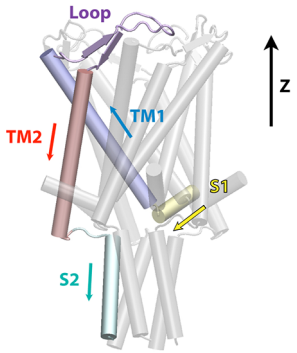

Figure 2. The structure of MscL. Rods show α-helices, and arrows show β-strands. One of the five chains is highlighted with colors to indicate the five structural segments. The arrows near the helices indicate their direction (N to C terminal). The z-axis (the surface normal vector) is added to indicate the orientation in the membrane.

chain consists of two transmembrane α-helices (TM1 and TM2), a loop, and two additional α-helices (S1 and S2). The trajectories were taken from ref 60, where all details of the molecular dynamics simulation and Hamiltonian construction are given. In short, we used a 2 ns long production run trajectory obtained after equilibration of the starting structure originating from the X-ray pdb file (2OAR).[47,61] The Hamiltonian parameters were constructed using the maps for the amide I vibration described in refs 52, 53, and 40 for the site frequencies, couplings, and transition dipoles. The transition polarizabilites ($\bar{\alpha}$) are used according to the model of Tsuboi.[39] This model accounts for the orientational dependence of the transition polarizability but neglects fluctuations induced by changes in the electrostatic environment. The transition dipoles and polarizabilities for the

dx.doi.org/10.1021/jp403111j | J. Phys. Chem. B 2013, 117, 6937−6945

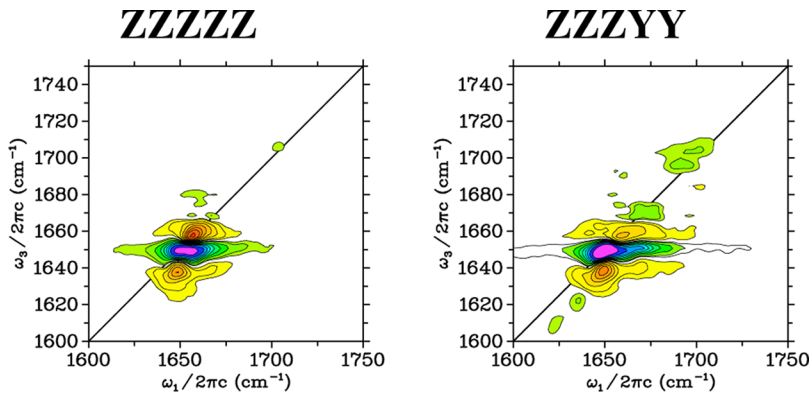

Figure 3. The *ZZZZZ* and *ZZZYY* lab frame polarization response functions for MscL for zero waiting time. The spectra are normalized to the maximum peak height for each polarization, and equidistant contours are used. Yellow to red colors indicate bleach in the upward direction and induced absorption in the downward direction. Green and blue colors indicate bleach in the downward direction and induced absorption in the upward direction.

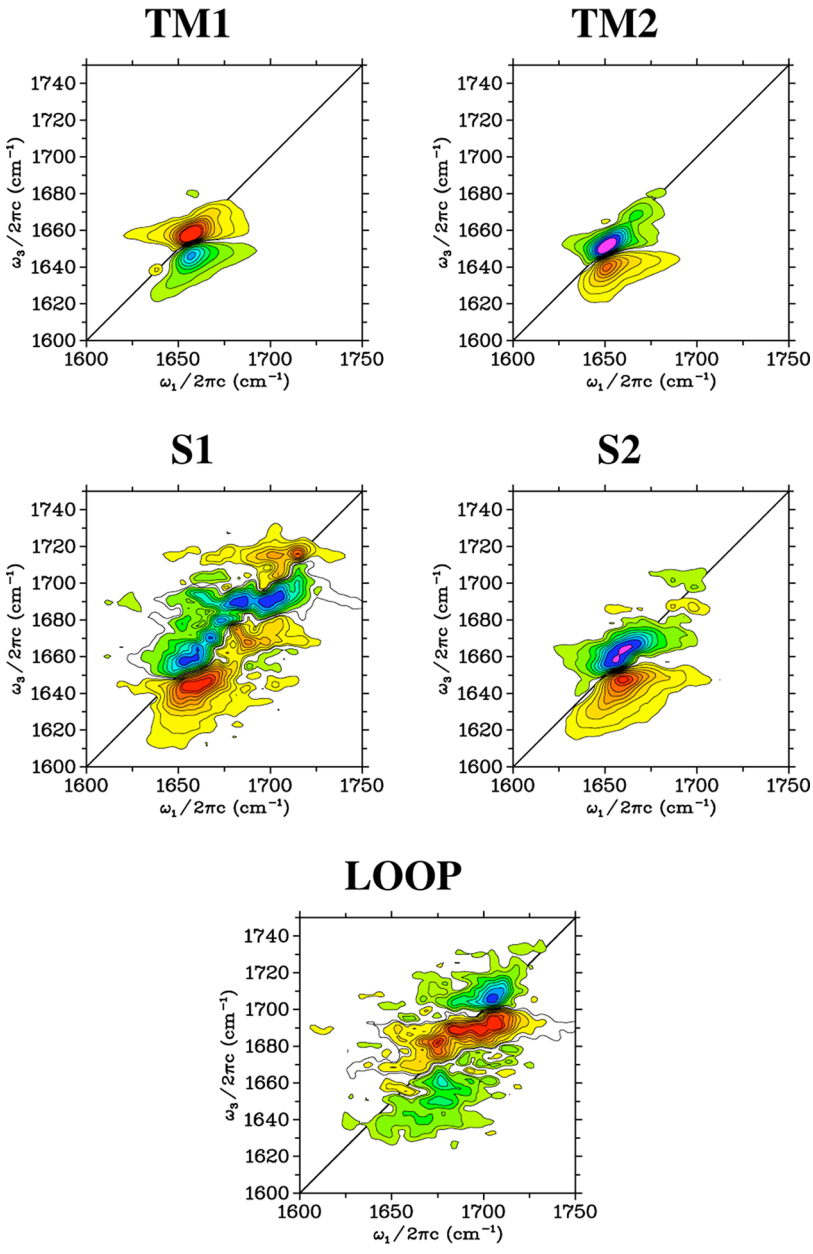

Figure 4. The *ZZZZZ* lab frame polarization response functions for the five structural segments of MscL. The spectra are normalized to the maximum peak height for each segment, and equidistant contours are used. Yellow to red colors indicate bleach in the upward direction and induced absorption in the downward direction. Green and blue colors indicate bleach in the downward direction and induced absorption in the upward direction.

dx.doi.org/10.1021/jp403111j | *J. Phys. Chem. B* 2013, 117, 6937−6945

sequence transitions are approximated using the harmonic approximation.[59] We will use a fixed anharmonicity of 16 cm^{-1}.[5]

The calculated response functions $\chi^{(4)}_{ZZZZZZ}$ and $\chi^{(4)}_{ZZZYY}$ for zero waiting time are shown in Figure 3. $\chi^{(4)}_{ZZZZZZ}$ is dominated by three peaks close to the diagonal at 1650 cm^{-1}. This is the region known to be related to α-helical structures.[62] In $\chi^{(4)}_{ZZZYY}$, a weak feature around 1700 cm^{-1} is observed as well. The spectra are better understood if we look at the spectra of the segments in Figures 4 and 5. The overall contribution of each segment is best seen in the diagonal slices in Figure 6. The largest segments, TM1 and TM2, are α-helices. They both give strong signals around 1650 cm^{-1} but with opposite sign. This sign difference is easily understood by the opposite direction of the two helices with respect to the surface normal. As the transition dipoles in a helix largely point in the same direction, the excitations on one helix will all have the same direction of the dominant transition dipoles. Therefore, the oppositely oriented helices giving a response with opposite sign as the response functions depends on an odd number of interactions with the laser field polarized in the Z-direction. As the signals of the two helices do not exactly coincide, the result is three peaks, where the ground state bleach and stimulated emission from TM1 results in the upper diagonal peak in red and yellow contours. The peak in the middle is caused by a combination of the TM1 excited state absorption signal that is shifted slightly below the diagonal and the ground state bleach and stimulated emission from TM2. The lowest peak results form the excited state absorption of TM2. The S2 segment points in the same direction as the TM2 segment and contributes in a similar way to the total spectrum, albeit with less intensity due to the smaller size. The small diagonal feature at 1700 cm^{-1} in the $\chi^{(4)}_{ZZZYY}$ response is most likely primarily originating from S2.

The response from the S1 and Loop segments are practically vanishing as compared to that of the other segments (see Figure 6).

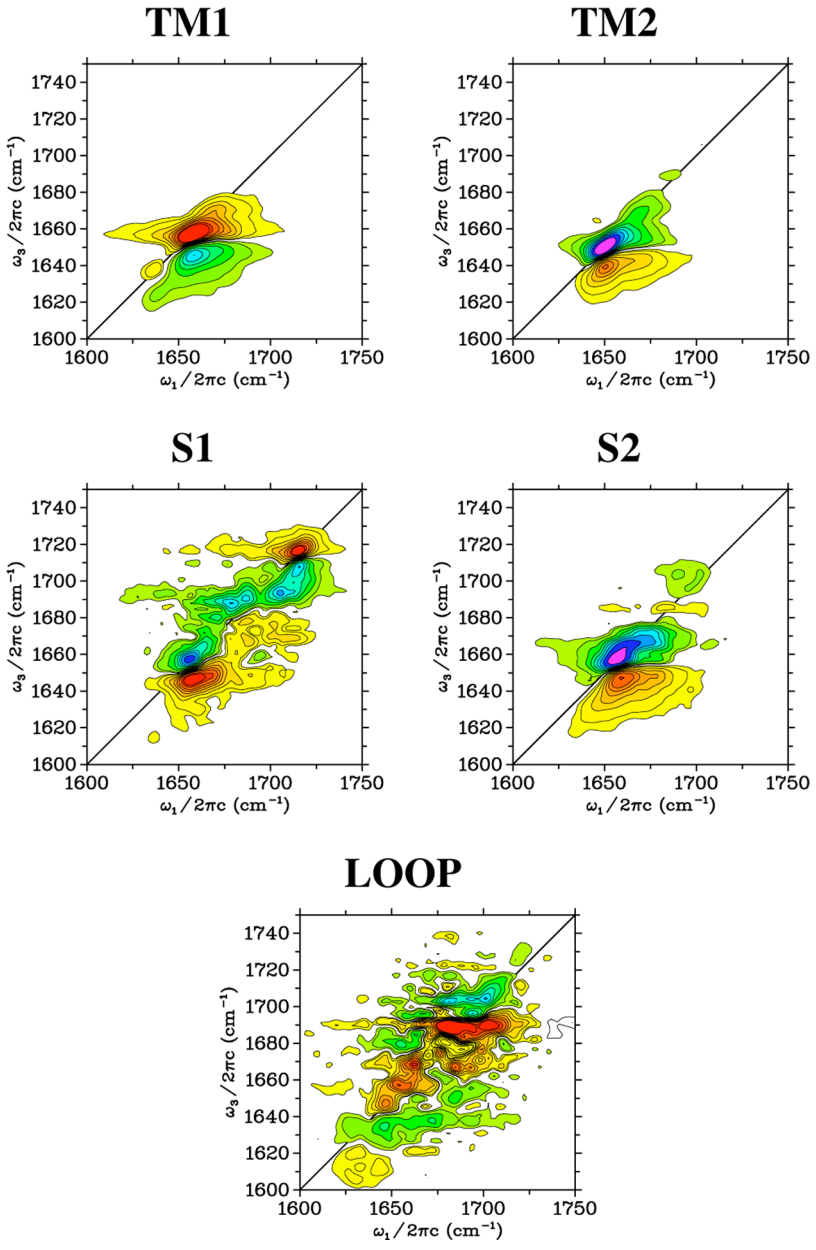

Figure 5. The *ZZZYY* lab frame polarization response functions for the five structural segments of MscL. The spectra are normalized to the maximum peak height for each segment, and equidistant contours are used. Yellow to red colors indicate bleach in the upward direction and induced absorption in the downward direction. Green and blue colors indicate bleach in the downward direction and induced absorption in the upward direction.

dx.doi.org/10.1021/jp403111j | J. Phys. Chem. B 2013, 117, 6937−6945

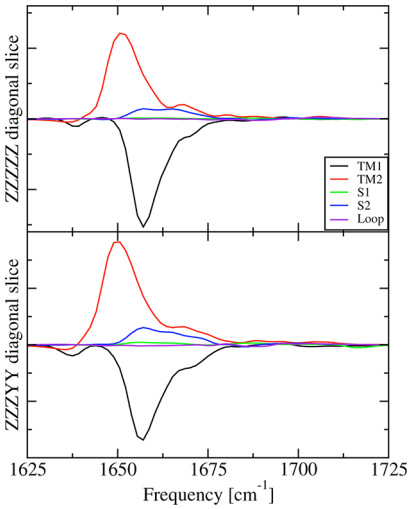

Figure 6. Slices along the diagonal of the 2DSFG spectra. The scales for the two polarization directions are optimized for better visibility and thus not comparable, but the relative intensities between the different segments with the same polarization direction are drawn to scale.

The response functions from these segments are much more complex and spectrally extended than that of TM1, TM2, and S2. In the S1 response, a feature that may originate from a downward pointing α-helix can be identified around 1650 cm^{-1}. However, at higher frequencies, signals from mostly downward pointing units can be seen as well. At 1720 cm^{-1}, a feature from an upward pointing unit is present. This is most evident in the $\chi^{(4)}_{ZZZYY}$ response. In the Loop response, the most prominent feature is above 1700 cm^{-1} in the $\chi^{(4)}_{ZZZZZ}$ response, while little distinctive features can be identified in the $\chi^{(4)}_{ZZZYY}$ response.

In all response functions, very few features that can be identified as cross-peaks are observed. The clearest ones are seen in the $\chi^{(4)}_{ZZZYY}$ response of S1, which constitutes only a small fraction of the total response. This lack of distinct cross-peaks can probably be partially attributed to the fact that the secondary structure is dominated by α-helices. In these cross-peaks have been identified in 2DIR;[63] however, the main peaks are only separated by about 10 cm^{-1} and thus not possible to disentangle without the use of special polarization directions. One may expect to see more distinct cross-peaks in systems containing more β-sheets.[64]

In Figure 7, the response functions are shown for an increased waiting time of 500 fs. The difference with the spectra obtained with zero waiting time is small. No clear cross-peaks have materialized as a sign of coupling between the TM1 and TM2 structures here either. The cross-peak enhancement with the use of increased waiting time has previously been proposed for 2DIR,[65] but here it does not appear to be applicable.

In the present study, we have disentangled the information in the total 2DSFG response by looking at different segments. It is important to emphasize that it is not given that the total response can be described as a simple sum of the response from the different segments. It has previously been shown that for 2DIR the response from different segments can approximately be added up to get the total response.[66] However, the very fine spectral details may be affected as communication between different structural elements is present.[37] In the present study, the segmentation was performed solely on the basis of the structural elements and not in an attempt to minimize the difference between the total response and that of the sum of the segment responses.

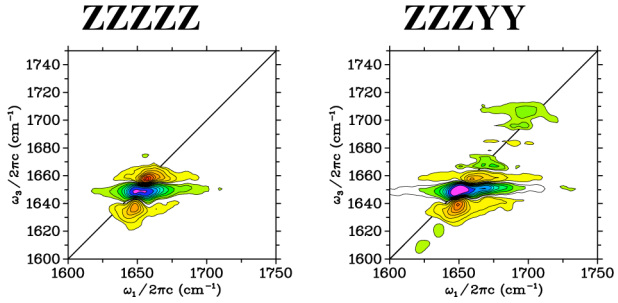

Figure 7. The *ZZZZZ* and *ZZZYY* lab frame polarization response functions for MscL for a 500 fs waiting time. The spectra are normalized to the maximum peak height for each polarization, and equidistant contours are used. Yellow to red colors indicate bleach in the upward direction and induced absorption in the downward direction. Green and blue colors indicate bleach in the downward direction and induced absorption in the upward direction.

DISCUSSION

The response functions presented in this paper are most directly connected with the heterodyne detected 2DSFG signals. With the homodyne detection technique, essentially the square of the response function is measured and phase information is lost. The initial 2DSFG experiments[3,4] used this simpler detection scheme. More recent studies have applied the heterodyne detection method,[22,24] and such experiments are thus feasible, albeit experimentally more challenging.

In the present simulations, we treated the rather idealized detection setup with glancing angle incidence of the laser beams. This is of course practically never achieved. A more realistic angle of incidence (typically in the range $40° < \gamma < 60°$) can be accounted for provided one has knowledge about the Fresnel factors present in the prefactors of eq 1 for the given interface. One will then need to simulate the complete set of laboratory frame response functions and combine these using eqs 1, 6, 7, and 8. Little is presently known about the Fresnel factors for the material of the present study. If they change slowly on changing the frequency they only influence weighting of the contribution of different lab frame response functions to the spectra. However, a recent study has shown that the Fresnel factors can significantly influence the shape of a normal SFG spectrum due to dispersion.[67] Such an effect may influence the spectral shapes significantly.

For small proteins and peptides, isotope editing[68−73] has been utilized to highlight particular peptide groups. This will also be possible to implement for 2DSFG. However, for the protein discussed in the present paper, it is unlikely to be of much use, as the signal from a single peptide bond is likely to be too weak to be separated from the background of the rest of the band. A more tractable strategy to obtain more detailed information will be to isotope label complete segments of proteins as previously done in 2DIR studies.[74] This will for example allow one to determine the orientational direction of a particular α-helix and of course confirm if a particular segment is indeed forming a helix or another secondary structure.

CONCLUSIONS

We have presented the extension of the NISE method to treat the calculation of 2DSFG response functions. The method was applied to the amide I region of a membrane protein. By calculating the response functions for segments of the whole structure, it was illustrated how different protein arrangements can be expected to manifest themselves in 2DSFG spectra. In particular, it was found that the orientation of the α-helices is manifested in the sign of their response, very much as one would expect from the knowledge of traditional SFG.

dx.doi.org/10.1021/jp403111j | J. Phys. Chem. B 2013, 117, 6937−6945

Since the 2DSFG technique is still in its infancy, there are still many things that we need to learn. The proper Fresnel factors neglected in this study and the optimal incidence angles need to be determined. While the mappings for the frequencies and transition dipoles are still under development, much less work has been done to find a proper choice of transition polarizabilities.

That said, with the present implementation, we have demonstrated that simulating 2DSFG response functions of large systems like proteins is possible by combining molecular dynamics simulations and ab *initio* based mappings for the Hamiltonian parameters. Furthermore, with the present study, we have shown that it will be worth the effort setting up 2DSFG experiments directed at the amide I band to experimentally study membrane bound proteins.

APPENDIX: POLARIZATION

The angle dependent prefactors A are given by

$$A_X(\Omega, \gamma, \omega) = \cos\Omega \cos\gamma L_{XX}(\omega) \quad (6)$$

$$A_Y(\Omega, \gamma, \omega) = \sin\Omega L_{YY}(\omega) \quad (7)$$

$$A_Z(\Omega, \gamma, \omega) = \cos\Omega \sin\gamma L_{ZZ}(\omega) \quad (8)$$

where L are the Fresnel coefficients representing the local field factors at the interface.[2,75] In practical experiments, Ω typically is either chosen to be polarized in the plane of the surface ($\Omega = 90°$) denoted s-polarization or perpendicular to the surface denoted p-polarization ($\Omega = 0°$). For an idealized setup, the angles of incidence γ are close to 90°, reflecting a glancing angle of incidence.

For the idealized setup using glancing angle incidence, eq 8 reduces to

$$A_X(0, 90, \omega) = 0 \quad (9)$$

$$A_Y(0, 90, \omega) = 0 \quad (10)$$

$$A_Z(0, 90, \omega) = L_{ZZ}(\omega) \quad (11)$$

for p-polarization and

$$A_X(90, 90, \omega) = 0 \quad (12)$$

$$A_Y(90, 90, \omega) = L_{YY}(\omega) \quad (13)$$

$$A_Z(90, 90, \omega) = 0 \quad (14)$$

for s-polarization.

Table 1. The Averaging Needed for Converting between the Lab Frame and Molecular Dynamics (MD) for a Sample Isotropic in the Surface Plane[a]

lab frame	MD frame	weight
$\chi^{(4)}_{ZZZZZ}$	$\chi^{(4)}_{zzzzz}$	1
$\chi^{(4)}_{ZZZYY}$	$\chi^{(4)}_{zzzxx}$	1/2
	$\chi^{(4)}_{zzzyy}$	1/2
$\chi^{(4)}_{YYZZZ}$	$\chi^{(4)}_{xxzzz}$	1/2
	$\chi^{(4)}_{yyzzz}$	1/2
$\chi^{(4)}_{YYZYY}$	$\chi^{(4)}_{xxzxx}$	3/12
	$\chi^{(4)}_{yyzyy}$	3/12
	$\chi^{(4)}_{yyzxx}$	1/12
	$\chi^{(4)}_{xxzyy}$	1/12
	$\chi^{(4)}_{yxzyx}$	1/12
	$\chi^{(4)}_{xyzxy}$	1/12
	$\chi^{(4)}_{yxzxy}$	1/12
	$\chi^{(4)}_{xyzyx}$	1/12

[a]The laser beams are assumed to move in the $X-Z$ plane.

Denoting the surface normal axis the Z/z-axis and assuming that the sample is isotropic in the $X-Y$ plane, the lab frame polarizations are obtained by averaging over the molecular dynamics frame according to Table 1. In systems with many identical chromophores as HOD in D_2O, one does not need this averaging, as typically one will average over a sufficient amount of random chromophore orientations. For large proteins that largely remain oriented the same way in the $x-y$ plane during a full molecular dynamics trajectory, such averaging is crucial. Only the lab frame polarization $\chi^{(4)}_{YYZYY}$ is given for configurations with one field in the Z direction. The weights for other polarizations with one field polarized in that direction can trivially be deduced from those of $\chi^{(4)}_{YYZYY}$. For samples isotopic in the $X-Y$ plane, polarization combinations with an even number of fields polarized along the Z-axis vanish.

AUTHOR INFORMATION

Corresponding Author

*E-mail: t.l.c.jansen@rug.nl.

Notes

The authors declare no competing financial interest.

ACKNOWLEDGMENTS

We are grateful to Martin Zanni for inspiring this work by sharing his theory paper on 2DSFG with us prior to publication.

REFERENCES

(1) Shen, Y. R. Surface Properties Probed by Second Harmonic and Sum-Frequency Generation. *Nature* **1989**, *337*, 519−525.

(2) Shen, Y. R. *The Principles of Nonlinear Optics*; John Wiley & Sons: New York, 1984.

(3) Bredenbeck, J.; Ghosh, A.; Smits, M.; Bonn, M. Ultrafast Two Dimensional-Infrared Spectroscopy of a Molecular Monolayer. *J. Am. Chem. Soc.* **2008**, *130*, 2152.

(4) Bredenbeck, J.; Ghosh, A.; Nienhuys, H.-K.; Bonn, M. Interface-Specific Ultrafast Two-Dimensional Vibrational Spectroscopy. *Acc. Chem. Res.* **2009**, *42*, 1332−1342.

(5) Hamm, P.; Lim, M. H.; Hochstrasser, R. M. Structure of the Amide I Band of Peptides Measured by Femtosecond Nonlinear-Infrared Spectroscopy. *J. Phys. Chem. B* **1998**, *102*, 6123.

(6) Hybl, J. D.; Albrecht, A. W.; Faeder, S. M. G.; Jonas, D. M. Two-Dimensional Electronic Spectroscopy. *Chem. Phys. Lett.* **1998**, *297*, 307−313.

(7) Hahn, E. L. Spin Echoes. *Phys. Rev.* **1950**, *80*, 580.

(8) Brixner, T.; Stenger, J.; Vaswani, H. M.; Cho, M.; Blankenship, R. E.; Fleming, G. R. Two-Dimensional Spectroscopy of Electronic Couplings in Photosynthesis. *Nature* **2005**, *434*, 625.

(9) Cahoon, J. F.; Sawyer, K. R.; Schlegel, J. P.; Harris, C. B. Determining Transition-State Geometries in Liquids Using 2D-IR. *Science* **2008**, *319*, 1820.

(10) Rubtsov, I. V. Relaxation-Assisted Two-Demensional Infrared (RA 2DIR) Method: Accessing Distances over 10 Å and Measuring Bond Connectivity Patterns. *Acc. Chem. Res.* **2009**, *42*, 1385−1394.

(11) King, J. T.; Baiz, C. R.; Kubarych, K. J. Solvent-Dependent Spectral Diffusion in Hydrogen Bonded "Vibrational Aggregate". *J. Phys. Chem. A* **2010**, *114*, 10590−10604.

(12) Fecko, C. J.; Eaves, J. D.; Loparo, J. J.; Tokmakoff, A.; Geissler, P. L. Ultrafast Hydrogen-Bond Dynamics in the Infrared Spectroscopy of Water. *Science* **2003**, *301*, 1698.

(13) Bredenbeck, J.; Helbing, J.; Nienhaus, G. U.; Hamm, P. Protein Ligand Migration Mapped by Nonequilibrium 2D-IR Exchange Spectroscopy. *Proc. Natl. Acad. Sci. U.S.A.* **2007**, *104*, 14243.

(14) Kim, Y. S.; Hochstrasser, R. M. Chemical Exchange 2D IR of Hydrogen-Bond Making and Breaking. *Proc. Natl. Acad. Sci. U.S.A.* **2005**, *102*, 11185.

(15) Jansen, T. L. C.; Cringus, D.; Pshenichnikov, M. S. Dissimilar Dynamics of Coupled Water Vibrations. *J. Phys. Chem. A* **2009**, *113*, 6260.
(16) Jansen, T. L. C.; Knoester, J. Waiting Time Dynamics in Two-Dimensional Infrared Spectroscopy. *Acc. Chem. Res.* **2009**, *42*, 1405−1411.
(17) Golonzka, O.; Khalil, M.; Demirdöven, N.; Tokmakoff, A. Coupling and Orientation between Anharmonic Vibrations Characterized with Two-Dimensional Infrared Vibrational Echo Spectroscopy. *J. Chem. Phys.* **2001**, *115*, 10814.
(18) Cheatum, C. M.; Tokmakoff, A.; Knoester, J. Signatures of Beta-Sheet Secondary Structures in Linear and Two-Dimensional Infrared Spectroscopy. *J. Chem. Phys.* **2004**, *120*, 8201.
(19) Fang, C.; Wang, J.; Charnley, A. K.; Barber-Armstrong, W.; Smith, A. B., III; Decatur, S. M.; Hochstrasser, R. M. Two Dimensional Infrared Measurements of the Coupling of Amide Modes of an α-Helix. *Chem. Phys. Lett.* **2003**, *382*, 586.
(20) Larsen, O. F. A.; Bodis, P.; Buma, W. J.; Hannam, J. S.; Leigh, D. A.; Woutersen, S. Probing the Structure of a Rotaxane with Two-Dimensional Infrared Spectroscopy. *Proc. Natl. Acad. Sci. U.S.A.* **2005**, *102*, 13378.
(21) Carter, J. A.; Wang, Z.; Dlott, D. D. Ultrafast Nonlinear Coherent Vibrational Sum-Frequency Spectroscopy Methods to Study Thermal Conductance of Molecules at Interfaces. *Acc. Chem. Res.* **2009**, *42*, 1343−1351.
(22) Xiong, W.; Laaser, J. E.; Mehlenbacher, R. D.; Zanni, M. T. Adding a Dimension to the Infrared Spectra of Interfaces using Heterodyne Detected 2D Sum-Frequency Generation (HD 2D SFG) Spectroscopy. *Proc. Natl. Acad. Sci. U.S.A.* **2011**, *108*, 20902−20907.
(23) Zhang, Z.; Piatkowski, L.; Bakker, H. J.; Bonn, M. Ultrafast Vibrational Energy Transfer at the Water/Air Interface Revealed by Two-Dimensional Surface Vibrational Spectroscopy. *Nature Chem.* **2011**, *3*, 888−893.
(24) Singh, P. C.; Nihonyanagi, S.; Yamaguchi, S.; Tahara, T. Ultrafast Vibrational Dynamics of Water at a Charged Interface Revealed by Two-Dimensional Heterodyne-Detected Vibrational Sum Frequency Generation. *J. Chem. Phys.* **2012**, *137*, 094706.
(25) Laaser, J. E.; Zanni, M. T. Extracting Structural Information from the Polarization Dependence of One- and Two-Dimensional Sum Frequency Generation Spectra. *J. Phys. Chem. A* **2013**, DOI: 10.1021/jp307721y.
(26) Ni, Y.; Gruenbaum, S.; Skinner, J. L. Slow Hydrogen-Bond Switching Dynamics at the Water Surface Revealed by Theoretical Two-Dimensional Sum-Frequency Spectroscopy. *Proc. Natl. Acad. Sci. U.S.A.* **2013**, *110*, 1992−1998.
(27) Liang, C.; Jansen, T. L. C. An Efficient N^3-Scaling Propagation Scheme for Simulating Two-Dimensional Infrared and Visible Spectra. *J. Chem. Theory Comput.* **2012**, *8*, 1706−1713.
(28) Jansen, T. L. C.; Knoester, J. Nonadiabatic Effects in the Two-Dimensional Infrared Spectra of Peptides: Alanine Dipeptide. *J. Phys. Chem. B* **2006**, *110*, 22910.
(29) Torii, H. Effects of Intermolecular Vibrational Coupling and Liquid Dynamics on the Polarized Raman and Two-Dimensional Infrared Spectral Profiles of Liquid N,N-Dimethylformamide Analysed with a Time-Domain Computational Method. *J. Phys. Chem. A* **2006**, *110*, 4822.
(30) Petersen, P. B.; Saykally, R. j. On the Nature of Ions at the Liquid Water Surface. *Annu. Rev. Phys. Chem.* **2006**, *57*, 333−364.
(31) Eisenthal, K. B. Liquid Interfaces Probed by Second-Harmonic and Sum-Frequency Spectroscopy. *Chem. Rev.* **1996**, *96*, 1343−1360.
(32) Wang, J.; Even, M. A.; Chen, X.; Schmaier, A. H.; Waite, J. H.; Chen, Z. Detection of Amide I Signals of Interfacial Proteins in Situ Using SFG. *J. Am. Chem. Soc.* **2003**, *125*, 9914−9915.
(33) Ye, S.; Li, H.; Wei, F.; Jasensky, J.; Boughton, A. P.; Yang, P.; Chen, Z. Observing a Model Ion Channel Gating Action in Model Cell Membranes in Real Time in Situ: Membrane Potential Chenge Induced Alamethicin Orientation Change. *J. Am. Chem. Soc.* **2012**, *134*, 6237−6243.
(34) Nguyen, K. T.; Le Clair, S. V.; Ye, S.; Chen, Z. Orientation Determination of Protein Helical Structures Using Linear and Nonlinear Vibrational Spectroscopy. *J. Phys. Chem. B* **2009**, *113*, 12169−12180.
(35) Krimm, S.; Abe, Y. Intermolecular Interaction Effects in amide I Vibrations of Beta Polypeptides. *Proc. Natl. Acad. Sci. U.S.A.* **1972**, *69*, 2788.
(36) Krimm, S.; Bandekar, J. Vibrationnal Spectroscopy and Conformation of Peptides and Proteins. *Adv. Protein Chem.* **1986**, *38*, 181.
(37) Karjalainen, E.-L.; Barth, A. Vibrational Coupling between Helices Influences the Amide I Infrared Absorption of Proteins: Application to Bacteriorhodopsin and Rhodopsin. *J. Phys. Chem. B* **2012**, *116*, 4448−4456.
(38) Unger, R.; Moult, J. Generic Algorithms for Protein Folding Simulations. *J. Mol. Biol.* **1993**, *231*, 75−81.
(39) Tsuboi, M.; Thomas, G. J. Raman Scattering Tensors in Biological Molecules and Their Assemblies. *Appl. Spectrosc. Rev.* **1997**, *32*, 263−299.
(40) Jansen, T. L. C.; Knoester, J. A Transferable Electrostatic Map for Solvation Effects on Amide I Vibrations and its Application to Linear and Two-Dimensional Spectroscopy. *J. Chem. Phys.* **2006**, *124*, 044502.
(41) Schmidt, J. R.; Corcelli, S. A.; Skinner, J. L. Ultrafast Vibrational Spectroscopy of Water and Aqueous N-methylacetamide: Comparison of Different Electronic Structure/Molecular Dynamics Approaches. *J. Chem. Phys.* **2004**, *121*, 8887.
(42) Hayashi, T.; Mukamel, S. Vibrational-Exciton Couplings for the Amide I, II, III, and A Modes of Peptides. *J. Phys. Chem. B* **2007**, *111*, 11032−11046.
(43) Ham, S.; Cho, M.; Amide, I. Modes in the N-Methylacetamide Dimer and Glycine Dipeptide Analog: Diagonal Force Constants. *J. Chem. Phys.* **2003**, *118*, 6915−6922.
(44) Gorbunov, R. D.; Kosov, D. S.; Stock, G. Ab initio-based Exciton Model of Amide I Vibrations in Peptides: Definition, Conformational Dependence, and Transferability. *J. Chem. Phys.* **2005**, *122*, 224904.
(45) Schmidt, J. R.; Corcelli, S. A.; Skinner, J. L. Pronounced Non-Condon Effects in the Ultrafast Infrared Spectroscopy of Water. *J. Chem. Phys.* **2005**, *123*, 044513.
(46) Kobus, M.; Gorbunov, R. D.; Nguyen, P. H.; Stock, G. Nonadiabatic Vibrational Dynamics and Spectroscopy of Peptides: A Quantum-Classical Description. *Chem. Phys.* **2008**, *347*, 208.
(47) Chang, G.; Spencer, R. H.; Lee, A. T.; Barclay, M. T.; Rees, D. C. Structure of the MscL Homolog from Mycobacterium Tuberculosis: a Gated Mechanosensitive Ion Channel. *Science* **1998**, *282*, 2220−2226.
(48) Perozo, E.; Cortes, D. M.; Sompornpisut, P.; Kloda, A.; Martinac, B. Open Channel Structure of MscL and the Gating Mechanism of Mechanosensitive Channels. *Nature* **2002**, *418*, 942.
(49) Yefimov, S.; van der Giessen, E.; Onck, P. R.; Marrink, S. J. Mechanosensitive Membrane Channels in Action. *Biophys. J.* **2008**, *94*, 2994−3002.
(50) Kocer, A.; Walko, M.; Meijberg, W.; Feringa, B. A Light-Actuated Nanovalve Derived from a Channel Protein. *Science* **2005**, *309*, 755−758.
(51) Mukamel, S. *Principles of Nonlinear Optical Spectroscopy*; Oxford University Press: New York, 1995.
(52) Jansen, T. L. C.; Dijkstra, A. G.; Watson, T. M.; Hirst, J. D.; Knoester, J. Modeling the Amide I Bands of Small Peptides. *J. Chem. Phys.* **2006**, *125*, 044312.
(53) Roy, S.; Lessing, J.; Meisl, G.; Ganim, Z.; Tokmakoff, A.; Knoester, J.; Jansen, T. l. C. Solvent and Conformation Dependence of Amide I Vibrations in Peptides and Proteins Containing Proline. *J. Chem. Phys.* **2011**, *135*, 234507.
(54) Auer, B. M.; Skinner, J. L. Vibrational Sum-Frequency Spectroscopy of the Water Liquid/Vapor Interface. *J. Phys. Chem. B* **2009**, *113*, 4125.
(55) Auer, B. M.; Skinner, J. L. Vibrational Sum-Frequency Spectroscopy of the Liquid/Vapor Interface for Dilute HOD in D2O. *J. Chem. Phys.* **2008**, *129*, 214705.

(56) Kwac, K.; Cho, M. H. Molecular Dynamics Simulation Study of N-Methylacetamide in Water. I. Amide I Mode Frequency Fluctuation. *J. Chem. Phys.* **2003**, *119*, 2247−2255.
(57) Gorbunov, R. D.; Stock, G. Ab Initio Based Building Block Model of Amide I Vibrations in Peptides. *Chem. Phys. Lett.* **2007**, *437*, 272.
(58) Bour, P.; Keiderling, T. A. Empirical Modeling of the Peptide Amide I Band IR Intensity in Water Solution. *J. Chem. Phys.* **2003**, *119*, 11253.
(59) Hamm, P.; Zanni, M. T. *Concepts and Methods of 2D Infrared Spectroscopy*; Cambridge University Press: Cambridge, U.K., 2011.
(60) Liang, C.; Louhivuori, M.; Marrink, S. J.; Jansen, T. L. C.; Knoester, J. Vibrational Spectra of a Machanosensitive Membrane Channel. *J. Phys. Chem. Lett.* **2013**, *4*, 448−452.
(61) Louhivuori, M.; Risselada, H. J.; van der Giessen, E.; Marrink, S. J. Release of Content through Mechano-Sensitive Gates in Pressurized Liposomes. *Proc. Natl. Acad. Sci. U.S.A.* **2010**, *16*, 19856−19860.
(62) Barth, A.; Zscherp, C. What Vibrations Tell Us about Proteins. *Q. Rev. Biophys.* **2002**, *35*, 369.
(63) Woutersen, S.; Hamm, P. Time-Resolved Two-Dimensional Vibrational Spectroscopy of a Short Alpha-Helix in Water. *J. Chem. Phys.* **2001**, *115*, 7737.
(64) Demirdöven, N.; Cheatum, C. M.; Chung, H. S.; Khalil, M.; Knoester, J.; Tokmakoff, A. Two-Dimensional Infrared Spectroscopy of Antiparallel Beta-Sheet Secondary Structure. *J. Am. Chem. Soc.* **2004**, *126*, 7981−7990.
(65) Jansen, T. L. C.; Knoester, J. Two-Dimensional Infrared Population Transfer Spectroscopy for Enhancing Structural Markers of Proteins. *Biophys. J.* **2008**, *94*, 1818−1825.
(66) Baiz, C. R.; Peng, C. S.; Reppert, M.; Jones, K. C.; Tokmakoff, A. Coherent Two-Dimensional Infrared Spectroscopy: Quantitative Analysis of Protein Secondary Structure in Solution. *Analyst* **2012**, *137*, 1739−1799.
(67) Backus, E. H. G.; Garcia-Araez, N.; Bonn, M.; Bakker, H. J. On the Role of Fresnel Factors in Sum-Frequency Generation Spectroscopy of Metal-Water and Metal-Ozide-Water Interfaces. *J. Phys. Chem. C* **2012**, *116*, 23351−23361.
(68) Woutersen, S.; Hamm, P. Isotope-Edited Two-Dimensional Vibrational Spectroscopy of Trialanine in Aqueous Solution. *J. Chem. Phys.* **2001**, *114*, 2727.
(69) Shim, S.-H.; Gupta, R.; Ling, Y. L.; Strasfeld, D. B.; Raleigh, D. P.; Zanni, M. T. Two-Dimensional IR Spectroscopy and Isotope Labeling Defines the Pathway of Amyloid Formation with Residue-Specific Resolution. *Proc. Natl. Acad. Sci. U.S.A.* **2009**, *106*, 6614.
(70) Smith, A. W.; Lessing, J.; Ganim, Z.; Peng, C. S.; Tokmakoff, A.; Roy, S.; Jansen, T. l. C.; Knoester, J. Melting of a Beta-Hairpin Using Isotope Label-Edited 2D IR Spectroscopy and Simulations. *J. Phys. Chem. B* **2010**, *114*, 10913−10924.
(71) Huang, R.; Setnicka, V.; Etienne, A.; Kim, J.; Kubelka, J.; Hammer, R. P.; Keiderling, T. A. Cross-Strand Coupling of a Beta-Hairpin Peptide Stabilized with an Aib-Gly Turn Studied Using Isotope-Edited IR Spectroscopy. *J. Am. Chem. Soc.* **2007**, *129*, 13592.
(72) Lessing, J.; Roy, S.; Reppert, M.; Baer, M. D.; Marx, D.; Jansen, T. l. C.; Knoester, J.; Tokmakoff, A. Identifying Residual Structure in Intrinsically Disordered Systems: A 2D IR Spectroscopic Study of the GVGXPGVG Peptide. *J. Am. Chem. Soc.* **2012**, *134*, 5032−5035.
(73) Manor, J.; Mukherjee, P.; Lin, Y.-S.; Leonov, H.; Skinner, J. L.; Zanni, M. T.; Arkin, I. T. Gating Mechanism of the Influenze a M2 Channel Revealed by 1D and 2D IR Spectroscopies. *Structure* **2009**, *17*, 247.
(74) Moran, S. D.; Woys, A. M.; Buchanan, L. E.; Bixby, E.; Decatur, S. M.; Zanni, M. T. Two-Dimensional IR Spectroscopy and Segmental C-13 Labeling Reveals the Domain Structure of Human Gamma D-Crystallin Amyloid Fibrils. *Proc. Natl. Acad. Sci. U.S.A.* **2012**, *109*, 3329−3334.
(75) Bloembergen, N.; Pershan, P. S. *Phys. Rev.* **1962**, *128*, 606−622.